引用格式：XU Da, WANG Xiaodan, SHU Zhengdong, et al. Structural and Luminescence Properties of Sm^{3+} and Eu^{3+} Co-doped GaN Thin Films[J]. Acta Photonica Sinica, 2026, 55(1):0131003
徐达,王晓丹,束正栋,等.Sm^{3+},Eu^{3+}共掺GaN薄膜的结构与发光特性[J].光子学报,2026,55(1):0131003

Sm^{3+},Eu^{3+}共掺GaN薄膜的结构与发光特性

徐达[1],王晓丹[1],束正栋[1],赵成伟[1],毛红敏[1],高晓冬[2],郑树楠[2],曾雄辉[2]
(1 苏州科技大学 物理科学与技术学院 江苏高校智能光电子器件与芯片重点实验室,苏州 215009)
(2 中国科学院苏州纳米技术与纳米仿生研究所,苏州 215123)

摘 要:为了探究Sm^{3+}离子对Eu^{3+}离子发光的调制作用,采用离子注入技术分别在GaN薄膜中实现了Sm^{3+}单掺杂及Sm^{3+}/Eu^{3+}共掺杂。通过高分辨率X射线衍射、拉曼光谱与阴极荧光等表征手段,系统研究了掺杂样品的晶体结构和发光特性。研究结果表明:随着Eu^{3+}掺杂浓度的增加,XRD衍射峰的半高宽呈现单调递增趋势,这表明样品的结晶质量逐渐下降。同时,晶格常数分析显示样品内部的压应力随Eu^{3+}剂量增加而增大。阴极荧光光谱分析表明存在Sm^{3+}向Eu^{3+}的能量传递:$^4G_{5/2}[Sm^{3+}]+{}^7F_0[Eu^{3+}]\rightarrow{}^6H_{5/2}[Sm^{3+}]+{}^5D_0[Eu^{3+}]$。进一步计算发现,$Sm^{3+}$主要通过电偶极-电偶极、电偶极-电四极共振方式将能量传递给Eu^{3+}。色度坐标随着Eu^{3+}的剂量增加从(0.527 5,0.369 5)变化到(0.606 3,0.353 2),发光颜色从黄红向深红转变,色温由1 580 K向730 K转变。

关键词:氮化镓;钕离子;能量传递;钐离子;阴极荧光
中图分类号:O472 **文献标识码**:A **doi**:10.3788/gzxb20265501.0131003

0 引言

GaN作为一种第三代宽禁带(3.4 eV)半导体材料,具备高电子迁移率、优异的热稳定性、低介电常数、高热导率、强化学惰性以及出色的抗辐照性能等优点[1]。相较于传统窄禁带半导体材料(如Si、GaAs),GaN基半导体在高功率、高频、高温及抗辐照等极端应用条件下展现出显著优势,已成为21世纪半导体技术发展的关键方向之一[2]。目前,GaN已被广泛应用于光电探测、高功率电子器件、高温高效紫外光电器件等领域[3-6]。

稀土元素因其独特的4f电子结构,表现出优异的光学、电学和磁学性能[7]。稀土离子(如Ce^{3+}至Yb^{3+})的4f电子受到外层$5s^2$和$5p^6$轨道的有效屏蔽,其能级受晶格环境影响较小,从而产生尖锐且与基质材料无关的特征发光[8]。在晶体场作用下,4f能级发生劈裂,原本禁戒的f-f跃迁得以部分解禁,从而产生独特而稳定的发射光谱[9]。

稀土离子掺杂可显著提升氮化镓(GaN)材料的光学性能。通过引入稀土离子特有的4f电子能级,可在GaN禁带中引入了高度局域化的新能级,促进光学跃迁,进而有效调控材料的发光特性[10]。该技术使得稀土掺杂GaN的光谱范围得以扩展,覆盖从紫外光到可见光乃至近红外的广泛区域,极大地增强了其在发光二极管(LED)显示技术、上转换及下转换等领域的应用潜力。

在具体稀土发光方面,Eu^{3+}的主要发光峰位于600 nm、622 nm、664 nm处,对应红光发射[11-13]。而Sm^{3+}的主要发光峰位于578 nm、618 nm、666 nm附近[25-27]。NGO N H等[14]在高质量Eu掺杂GaN薄膜中观测到光学增益现象。PERES M等[15]发现,将Eu掺杂GaN/AlN量子点在1 000 ℃至1 200 ℃下退火,能有效激活Eu^{3+}发光中心并增强发光强度,但对其所处的局域晶体场环境无明显影响。

基金项目:国家自然科学基金(61974158),江苏省自然科学基金(BK20221263),江苏省“十四五”光学工程重点学科项目(2021135)
第一作者:徐达,1978378223@qq.com
通讯作者:王晓丹,xiaodanwang@mail.usts.edu.cn
收稿日期:2025-08-25;**录用日期**:2025-10-29

LANG Jihui等[16]研究Sm^{3+}和Eu^{3+}在共掺ZnO体系，发现Sm^{3+}可以有效提高Eu^{3+}的发光强度。Sm^{3+}和Eu^{3+}共掺杂样品可以提高能量转移效率，Sm^{3+}可作为敏化剂，通过非辐射能量转移机制将激发能传递给Eu^{3+}，从而增强Eu^{3+}的红色发光[17]。PAVITRA E等[18]研究表明Sm^{3+}和Eu^{3+}共掺杂，通过调控Tb^{3+}/Eu^{3+}或Tb^{3+}/Sm^{3+}的浓度和激发波长，实现了发光颜色从绿色、橙色到白色的连续可调谐。

目前，针对Sm^{3+}/Eu^{3+}共掺GaN体系研究尚属探索阶段。当前InGaN基红光LED所面临的固有挑战在于：为实现红光发射所需的高铟(In)组分极易引发相分离，导致器件效率与稳定性下降[19]。相比之下，Eu^{3+}等稀土离子在GaN中能产生色纯度极高的稳定红光，是一条有希望的技术路线。本研究通过引入Sm^{3+}进行共掺，旨在探究其对Eu^{3+}发光中心的调制作用，为开发一种新型红光实现方案提供了实验依据，该方案有望替代高In组分InGaN，并与现有GaN半导体工艺保持更高兼容性。

为了系统探究Sm^{3+}，Eu^{3+}共掺GaN(GaN∶Sm，Eu)的微观结构与发光特性，本文采用离子注入技术在GaN薄膜中引入Sm^{3+}，并借助高温退火处理实现稀土离子的光学激活。样品的晶格应力状态通过高分辨率X射线衍射仪(High-Resolution X-Ray Diffraction，HRXRD)和拉曼光谱(Raman Spectroscopy)进行分析，并通过光致发光(Photoluminescence Spectroscopy，PL)和阴极荧光(Cathodoluminescence Spectroscopy，CL)表征材料的发光特性。

1 实验过程

实验所用的GaN薄膜采用金属有机物化学气相沉积(MOCVD)方法在(0001)面蓝宝石衬底上制备，薄膜厚度约为4 μm。Sm^{3+}和Eu^{3+}通过LC-4型离子注入机注入。首先进行Sm^{3+}单掺杂实验；Sm^{3+}和Eu^{3+}共掺杂时，固定Sm^{3+}剂量，变化Eu^{3+}的注入剂量，样品具体注入参数如表1所示。在注入能量为200 keV、方向偏离法线7°的条件下，离子注入角度是决定Sm^{3+}和Eu^{3+}在GaN中分布情况的关键因素。在离子注入过程中，由于注入剂量相对较低，注入离子主要分布在近表面区域，导致样品近表面晶体结构受损并产生大量缺陷。为了恢复晶格损伤，所有样品均在氨气气氛中、1 000 ℃下退火处理1 h。

表1 GaN∶Sm^{3+}与GaN∶Sm^{3+}，Eu^{3+}样品的离子注入剂量参数

Table 1 Ion implantation dose parameters for GaN∶Sm^{3+} and GaN∶Sm^{3+}, Eu^{3+}samples

Sample	Sm^{3+}/(at·cm^{-2})	Eu^{3+}/(at·cm^{-2})
GaN∶Sm^{3+}	1×10^{14}	—
GaN∶Sm^{3+}	5×10^{14}	—
GaN∶Sm^{3+}	1×10^{15}	—
GaN∶Sm^{3+}，Eu^{3+}	5×10^{14}	1×10^{14}
GaN∶Sm^{3+}，Eu^{3+}	5×10^{14}	5×10^{14}
GaN∶Sm^{3+}，Eu^{3+}	5×10^{14}	1×10^{15}

在结构特性方面，分别对样品进行HRXRD和拉曼光谱测试；在光学表征方面，分别进行PL和CL测试。本实验使用德国Bruker公司D8 Discover高分辨衍射仪进行HRXRD测试，该仪器配备Ge(440)四晶单色器，X光发散角≤12″，采用Cu $K\alpha_1$射线(波长0.154 nm)。拉曼光谱测试在LABRAM HR 800型激光共聚焦拉曼光谱仪上进行，激发光源为325 nm He-Cd激光器。PL光谱在LabRAM HR800型光谱仪的PL模式下采集，激发光源为325 nm He-Cd激光器，激光功率28 mW。CL光谱在配备MonoCL3+阴极发光附件的Quanta 400 FEG型场发射扫描电子显微镜(SEM)上采集。

2 结果与讨论

2.1 X射线衍射和Raman的结构表征

离子注入引入的缺陷会导致晶体结构发生显著变化，引起衍射峰半高宽展宽。该展宽效应主要源于三种机制：位错引起晶格局部扭曲，破坏长程有序性；位错周围应变场导致布拉格衍射角分布展宽；高缺陷浓度区域形成位错墙，将晶体分割为多个微小晶畴，从而减小有效晶粒尺寸。这些微观结构变化共同导致X射线衍射谱线明显宽化[16]。图1(a)是Sm^{3+}单掺GaN的(0002)面的晶体摇摆曲线，随着Sm^{3+}的注入剂量从1×10^{14} at/cm^{2}增加至1×10^{15} at/cm^2，半高宽由187.3 arcsec增大至204.4 arcsec，表明晶体质量随Sm^{3+}浓度增

加而降低，Sm^{3+}的注入引入了新的缺陷。当Sm^{3+}浓度为1×10^{15} at/cm^{2}时，晶体损伤最为严重。图1(b)为固定Sm^{3+}剂量(5×10^{14} at/cm^2)时，不同Eu^{3+}注入剂量下GaN的(0002)面的晶体摇摆曲线。随着Eu^{3+}注入剂量的增加，摇摆曲线半高宽呈现先减小后增大的趋势，在注入剂量为5×10^{14} at/cm^{2}时，可能引入了较低浓度的点缺陷或微小晶格畸变，这些缺陷对晶格长程有序性影响较小，甚至可能起到一定的“退火”作用，使衍射峰略微锐化[20]。这种微小的晶格畸变可能与点缺陷的引入有关，其在低剂量下对衍射峰的展宽影响较小，反而可能使衍射峰变得更加尖锐，从而导致半高宽略有减小。随着注入剂量进一步增加，半高宽开始增大，并在Eu^{3+}剂量为1×10^{15} at/cm^{2}时达到最大值。

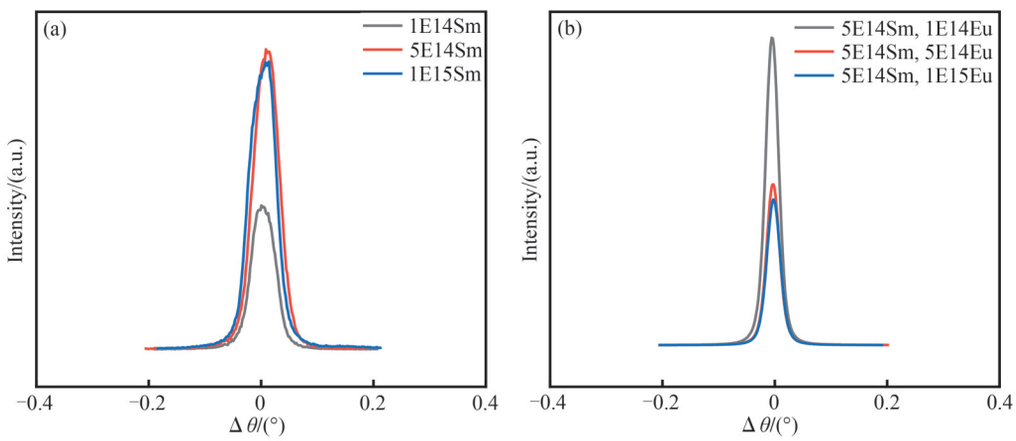


图1 GaN:Sm^{3+}与GaN:Sm^{3+}，Eu^{3+}的(0002)晶面摇摆曲线。(a) GaN:Sm^{3+}的(0002)晶面摇摆曲线(半高宽值：1E14Sm = 187.3 arcsec；5E14Sm = 198.9 arcsec；1E15Sm = 204.4 arcsec)；(b) GaN:Sm^{3+}，Eu^{3+}的(0002)晶面摇摆曲线(半高宽值：5E14Sm，1E14Eu = 252.8 arcsec；5E14Sm，5E14Eu = 248.0 arcsec；5E14Sm，1E15Eu = 257.9 arcsec)

Fig. 1 Rocking curves of the (0002) plane for GaN:Sm^{3+} and GaN:Sm^{3+}, Eu^{3+}. (a) Rocking curve for GaN:Sm^{3+} (FWHM values: 1×10^{14} Sm = 187.3 arcsec; 5×10^{14} Sm = 198.9 arcsec; 1×10^{15} Sm = 204.4 arcsec); (b) Rocking curve for GaN:Sm^{3+}, Eu^{3+} (FWHM values: 5×10^{14} Sm, 1×10^{14}Eu = 252.8 arcsec; 5×10^{14} Sm, 5×10^{14} Eu = 248.0 arcsec; 5×10^{14} Sm, 1×10^{14}Eu = 257.9 arcsec)

为分析晶体中的应力变化，对GaN(0002)晶面进行了X射线衍射测试，结果如图2所示。根据布拉格衍射定律 $n\lambda=2d\sin\theta$ 可知，当注入剂量从1×10^{14} at/cm^{2}增加至5×10^{14} at/cm^{2}时，衍射角减小，晶面间距d增大，表明晶格发生膨胀，对应压应力状态。然而，当剂量从5×10^{14} at/cm^{2}继续增加至1×10^{15} at/cm^{2}时，衍射角略有回升，晶格中的压应力得到部分释放。但在Sm^{3+}/Eu^{3+}共掺GaN样品中观察到相反趋势：随Eu^{3+}剂量增加，衍射角持续减小，d值上升，晶格膨胀加剧，压应力进一步增强。

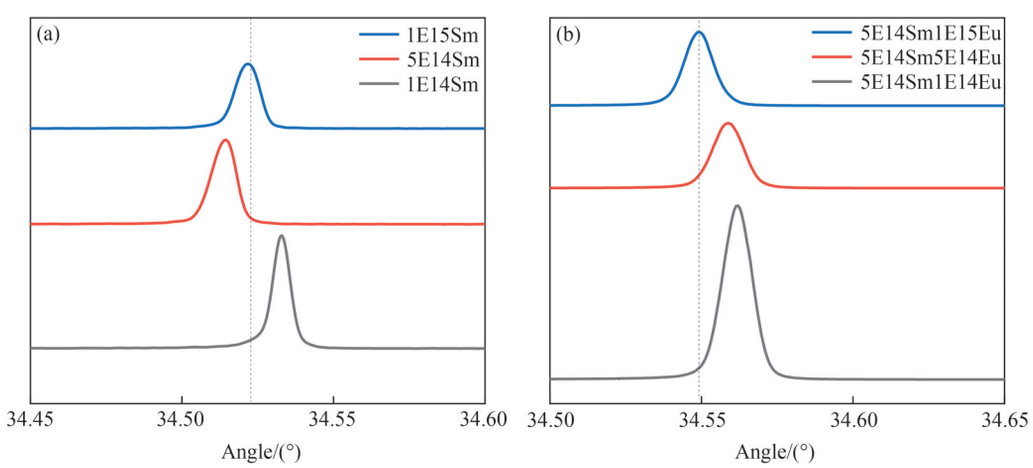


图2 GaN:Sm^{3+}与GaN:Sm^{3+}，Eu^{3+}的(0002)晶面三轴2θ/ω衍射谱图。(a) GaN:Sm^{3+}样品；(b) GaN:Sm^{3+}，Eu^{3+}共掺样品

Fig. 2 Triple-axis 2θ/ω diffraction patterns of the (0002) plane for GaN:Sm^{3+} and GaN:Sm^{3+}, Eu^{3+}. (a) GaN:Sm^{3+} sample; (b) GaN:Sm^{3+}, Eu^{3+} co-doped sample

为验证XRD的应力分析结果，对这批样品做了拉曼光谱的测试，图3(a)是GaN:Sm^{3+}的拉曼光谱，其中143 cm^{-1}、571 cm^{-1}和736 cm^{-1}处的拉曼峰分别对应于E_2^{low}声子模、E_2^{high}声子模和A_1(LO)声子模[21]。未受应变的GaN的E_2^{high}声子模特征频率约为568 cm^{-1}[22-23]。本研究中观察到的微小拉曼位移差异表明GaN与衬底之间的应力变化较小，晶格失配现象几乎可忽略。E_2^{high}模频率蓝移通常表明材料内部存在面内压应力(in-plane compressive stress)，而红移则对应面内张应力(in-plane tensile stress)[24]。图3(b)是GaN:Sm^{3+} E_2^{high}声子模的放大图，由3(b)可知随着Sm^{3+}浓度的增加E_2^{high}声子模的拉曼位移变化不大，但与标准的相比，Sm^{3+}掺杂GaN样品表现为张应力。

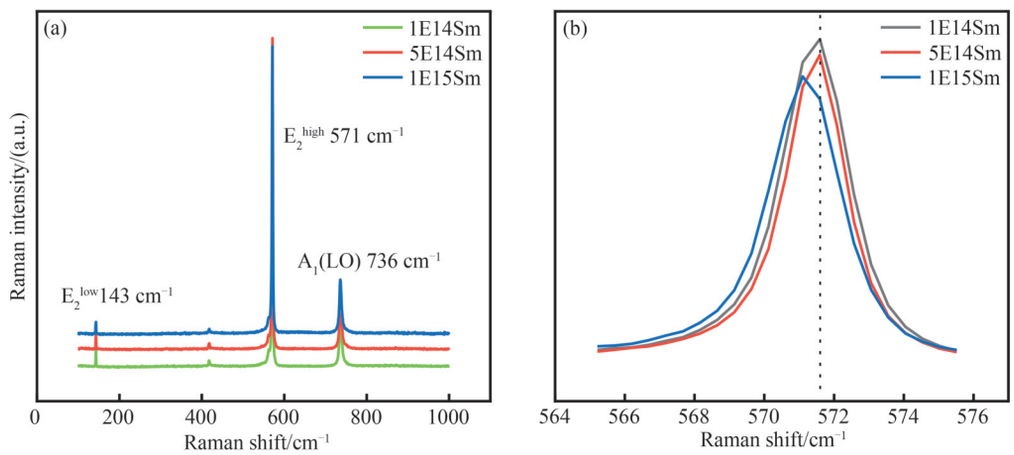


图3 GaN:Sm^{3+}的拉曼光谱图。(a) 显示E_2^{low}、E_2^{high}和A_1(LO)声子模的完整拉曼光谱；(b) E_2^{high}声子模区域的放大图

Fig. 3 Raman spectra of GaN:Sm^{3+}. (a) Full Raman spectrum showing E_2^{low}, E_2^{high}, and A_1(LO) phonon modes; (b) Magnified view of the E_2^{high} phonon mode region

图4(a)是GaN:Sm^{3+},Eu^{3+}的拉曼光谱，其中143 cm^{-1}、570 cm^{-1}和736 cm^{-1}处的拉曼峰分别对应于E_2^{low}声子模、E_2^{high}声子模和A_1(LO)声子模。图4(b)是GaN:Sm^{3+},Eu^{3+} E_2^{high}声子模的放大图，其峰位基本不随Eu^{3+}剂量变化，但与单掺样品比较明显向高频移动(蓝移)，说明Eu^{3+}的注入导致样品压应力增大。

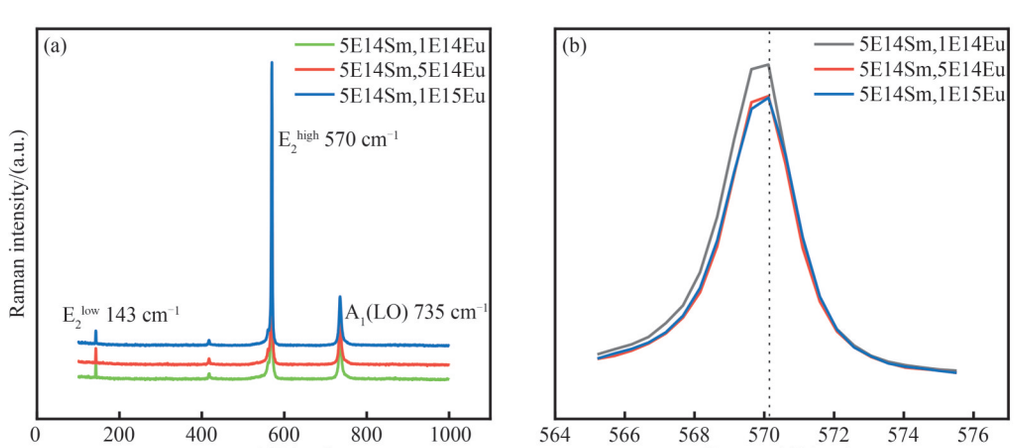


图4 GaN:Sm^{3+}, Eu^{3+}的拉曼光谱图。(a) 显示E_2^{low}、E_2^{high}和A_1(LO)声子模的完整拉曼光谱；(b) E_2^{high}声子模区域的放大图

Fig. 4 Raman spectra of GaN: Sm^{3+}, Eu^{3+}. (a) Full Raman spectrum showing E_2^{low}, E_2^{high}, and A_1(LO) phonon modes; (b) Magnified view of the E_2^{high} phonon mode region

2.2 光学特性

图5是Sm^{3+}单掺GaN样品的CL光谱。Sm^{3+}的特征发射峰主要位于565 nm，615 nm，668 nm，705 nm，分别对应Sm^{3+}的$^4G_{5/2}\rightarrow{}^6H_{5/2}$，$^4G_{5/2}\rightarrow{}^6H_{7/2}$，$^4G_{5/2}\rightarrow{}^6H_{9/2}$，$^4G_{5/2}\rightarrow{}^6H_{7/2}$的跃迁[25-28]。在图5(a)中可以观察到$Sm^{3+}$在577 nm，618 nm，666 nm附近存在Sm^{3+}的发光峰，分别对应Sm^{3+}的$^4G_{5/2}\rightarrow{}^6H_{5/2}$，$^4G_{5/2}\rightarrow{}^6H_{7/2}$，$^4G_{5/2}\rightarrow{}^6H_{9/2}$的跃迁。

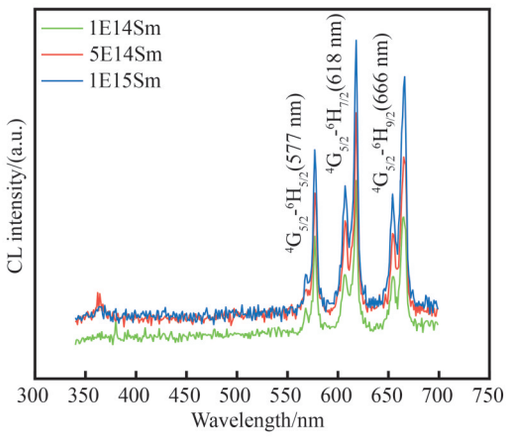


图5　GaN：Sm^{3+} Cl光谱图

Fig. 5　CL spectrum of GaN：Sm^{3+}

图6(a)是GaN：Sm^{3+}，Eu^{3+}样品的CL光谱。可见共掺的样品中Eu^{3+}的发光峰比较强，Sm^{3+}的发光峰比较弱，仅在578 nm附近观察到较弱的Sm^{3+}发射峰，对应Sm^{3+}的$^4G_{5/2}\rightarrow{}^6H_{5/2}$的跃迁。$Eu^{3+}$的特征发射峰位于543 nm，587 nm，600 nm，620 nm，663 nm附近，分别对应Eu^{3+}的$^5D_1\rightarrow{}^7F_1$，$^5D_0\rightarrow{}^7F_0$，$^5D_0\rightarrow{}^7F_1$，$^5D_0\rightarrow{}^7F_2$，$^5D_0\rightarrow{}^7F_3$的跃迁[11-13]。图6(b)是Sm^{3+}和Eu^{3+}最强发光峰(分别位于～577 nm和～620 nm)的积分强度随Eu^{3+}剂量变化的关系。可见随着Eu^{3+}的剂量增加，Eu^{3+}在620 nm处发光强度持续增强，而Sm^{3+}的577 nm发光强度持续减弱，这种此消彼长的变化可归因于Sm^{3+}从$^4G_{5/2}$能级的发射与Eu^{3+}的多个吸收跃迁存在光谱重叠，表明Sm^{3+}与Eu^{3+}之间存在明显的能量传递过程。

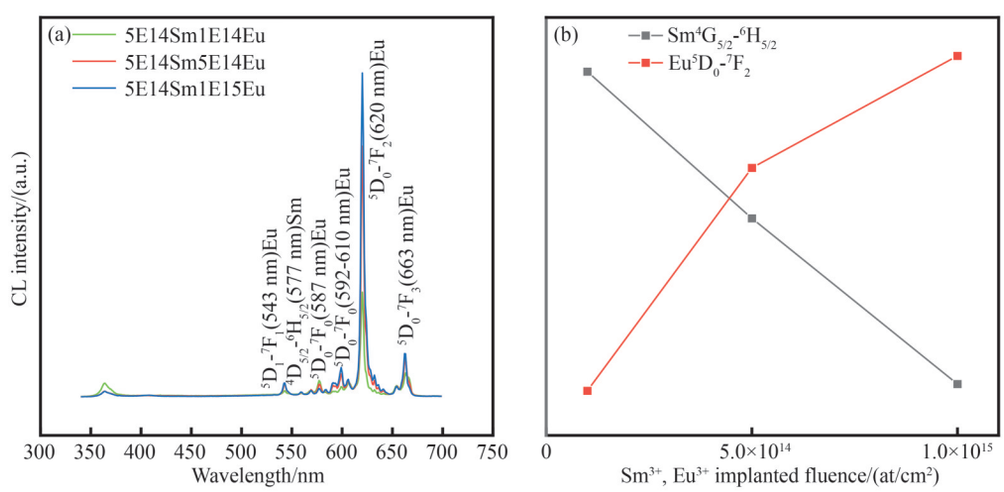


图6　GaN：Sm^{3+}，Eu^{3+}共掺样品的阴极荧光(CL)光谱及发射强度分析。(a)显示Sm^{3+}和Eu^{3+}特征发射的CL光谱；(b)Sm^{3+}(～577 nm)和Eu^{3+}(～620 nm)最强发射峰的积分强度随Eu^{3+}注入剂量的变化关系

Fig. 6　Cathodoluminescence (CL) spectra and emission intensity analysis of GaN：Sm^{3+}, Eu^{3+}. (a) CL spectra showing the characteristic emissions of $Sm^{3+}$and Eu^{3+}; (b) Variation of the integrated emission intensities for the strongest peaks of Sm^{3+} (～577 nm) and Eu^{3+} (～620 nm) as a function of Eu^{3+} implantation dose

值得注意的是，该能量转移过程的主导机制并非依赖于Eu^{3+}离子固有的、基于Laporte选择定则弱允许的$^7F_0\rightarrow{}^5D_0$电偶极跃迁的微小吸收截面，而是源于供体-受体对之间高度共振的能级匹配。具体而言，Sm^{3+}离子的$^4G_{5/2}\rightarrow{}^6H_{5/2}$辐射跃迁能与$Eu^{3+}$离子的$^7F_0\rightarrow{}^5D_0$能级差形成近乎完美的谱线匹配，从而构成了一个高效的Förster型共振能量转移通道[36]。Sm^{3+}与Eu^{3+}之间的能量传递主要通过$^4G_{5/2}\rightarrow{}^5D_0$路径实现，这得益于两者能级的高度匹配与极高的共振能量转移效率[35]。此外，能量也可转移至Eu^{3+}的更高能级(如$^5D_2$、$^5L_6$)，再通过非辐射弛豫至$^5D_0$发光，但该途径并非主要能量传递路径。

在能量传递过程中，供体(Sm^{3+})与受体(Eu^{3+})之间的能量转移效率主要由光谱重叠程度和离子间的距

离等决定。为了探究Sm^{3+}和Eu^{3+}之间的作用机制，需估算离子间的临界传递距离。本文采用基于Dexter交换作用的公式估算临界距离R_c[11,28-29]。

$$R_c = 2\left(\frac{3V}{4\pi C_p N}\right)^{\frac{1}{3}} \tag{1}$$

式中，R_c为Eu^{3+}和Sm^{3+}之间的平均距离，V为原胞体积（取0.045 9 nm^3），C_p为Eu^{3+}和Sm^{3+}的总浓度，N为原胞中的阳离子数目（取2）。本文通过模拟仿真方法对掺杂浓度进行估算，从而定量分析能量转移过程中的离子间距效应。估算方法为

$$N_p = \frac{\phi_i}{\Delta R_p (2\pi)^{\frac{1}{2}}} \approx \frac{0.4\phi_i}{\Delta R_p} \tag{2}$$

$$C_p = \frac{N_p}{N_p + N_t} \tag{3}$$

式中，N_p为注入Eu^{3+}和Sm^{3+}的总数（at/cm^3），ϕ_i是总离子注入计量（at/cm^2），ΔR_p为注入离子的分布深度范围（通过SRIM软件模拟得到约为15.5 nm），N_t为GaN中的Ga的原子密度（约4.357×10^{22} at/cm^2）。

固定Sm^{3+}浓度为5×10^{14} at/cm^2，Eu^{3+}的浓度分别为1×10^{14} at/cm^2，5×10^{14} at/cm^2，1×10^{15} at/cm^2时，估算得到的C_p以及R_c的值如表2所示。

表2 C_p以及R_c的值的计算结果

Table 2 Calculation results of average injection dose C_p and critical distance R_c

Sm^{3+}/($at\cdot cm^{-2}$)	Eu^{3+}/($at\cdot cm^{-2}$)	C_p/(%, atom fraction)	R_c/nm
5×10^{14}	1×10^{14}	0.353 188	2.243 84
5×10^{14}	5×10^{14}	0.587 263	1.894 01
5×10^{14}	1×10^{15}	0.878 316	1.656 19

稀土离子间的距离一般小于0.5 nm时才能够发生能量传递[34]，共振能量传递（Resonance Energy Transfer，RET）是指激发态供体（Donor，D）通过非辐射方式将能量传递给受体（Acceptor，A）的过程，其核心机制是电磁耦合或电子交换，无须光子参与。能量传递机制可能涉及电多极相互作用（偶极-偶极、偶极-四极、四极-四极）或交换相互作用[31]。

根据Dexter多极子能量传递理论与Reisfeld近似理论，进一步分析Sm^{3+}与Eu^{3+}之间的电多极子相互作用，其关系式可表示为[35]

$$\frac{I_0}{I} = C_P^{n/3} \tag{4}$$

式中，I_0与I分别表示掺杂Eu^{3+}前后Sm^{3+}的发光强度；参数n取值6、8和10时，分别对应电偶极-电偶极、电偶极-电四极以及电四极-电四极相互作用类型。本文选取CL光谱中Eu^{3+}在$^5D_0\rightarrow{}^7F_2$跃迁处发光峰的积分强度进行拟合分析，结果如图7所示。当n分别取6、8和10时，决定系数R^2（反映拟合优度，越接近1表示拟合越好）依次为0.998 84、0.995 69和0.972 81。在n=6、8时获得拟合效果较好且相近，表明在Sm^{3+}、Eu^{3+}共掺的GaN材料中，Sm^{3+}与Eu^{3+}之间的能量传递以电偶极-电偶极、电偶极-电四极相互作用为主导机制。

图8是Eu^{3+}和Sm^{3+}的能量传递机制图，在电子束激发下，处于基态（$^6H_{5/2}$）的Sm^{3+}离子吸收辐射能量后跃迁至$^6G_{11/2}$激发态。随后，这些激发态电子通过非辐射弛豫过程（NR）转移至中间能级$^4G_{5/2}$。最终，电子从$^4G_{5/2}$能级向低能态^6H_J（J=5/2、7/2、9/2、11/2）跃迁时，会释放特征光子，在577 nm、618 nm、及666 nm处产生Sm^{3+}离子的特征发射光谱[32]。Sm^{3+}的$^4G_{5/2}\rightarrow{}^6H_{5/2}$的跃迁（能级差约为2.217 eV）与$Eu^{3+}$的$^5D_0\rightarrow{}^7F_0$的跃迁（能级差约为2.143 eV），二者的能级差相差仅为74 meV，而与Eu^{3+}的$^5D_1\rightarrow{}^7F_0$的跃迁（能级差约为2.335 eV）相差为118 meV，前者（74 meV）能级匹配度更优，因此能量转移概率最大。表明Sm^{3+}和Eu^{3+}主要通过前者路径发生共振能量转移。由于Sm^{3+}的$^4G_{5/2}$的能级与Eu^{3+}的$^5D_0$能级差（99 meV）比Sm^{3+}的$^4G_{5/2}$的能级与Eu^{3+}的$^5D_1$能级差小（130 meV），因此能量传递是Sm^{3+}（$^4G_{5/2}$）→Eu^{3+}

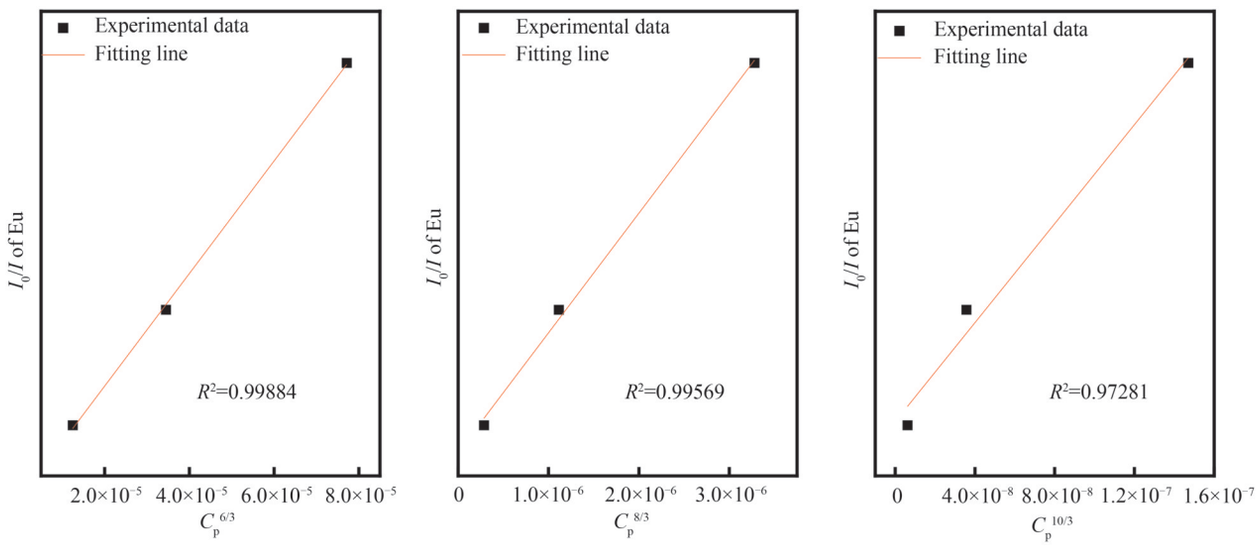


图 7　GaN:Sm^{3+}:Eu^{3+} 样品中 Eu 的 I_0/I 与 $C_p^{n/3}$ 的函数关系

Fig. 7　The relationship between I_0/I of Eu and $C_p^{n/3}$ in the GaN: Sm^{3+}:Eu^{3+} sample

($^5D_0$) 的声子俘获概率更高[33]。Sm^{3+}与Eu^{3+}的能量传递过程可表述为：$^4G_{5/2}[Sm^{3+}] + {}^7F_0[Eu^{3+}] \rightarrow {}^6H_{5/2}[Sm^{3+}] + {}^5D_0[Eu^{3+}]$。

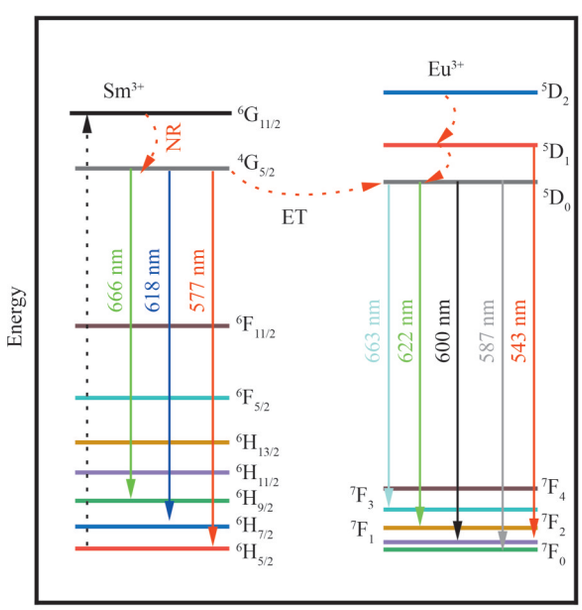


图 8　Sm^{3+}与Eu^{3+}的能级跃迁图

Fig. 8　Energy level transition diagram of Sm^{3+} and Eu^{3+}

图 9 为不同Eu^{3+}注入剂量下 GaN:Sm^{3+}，Eu^{3+}样品的色度坐标图，利用 McCamy 的近似公式(5)进行计算[34]。

$$CCT = -449n^3 + 3\,525n^2 - 6\,823n + 5\,520.33 \tag{5}$$

式中，$n=(x-x_e)/(y-y_e)$，n 为斜率的倒数，$x_e=0.332$，$y_e=0.186$。由色度坐标进一步计算相关色温(CCT)，计算结果如表 3 所示。随着Eu^{3+}的浓度从 1×10^{14} at/cm^{2}增加到 1×10^{15} at/cm^{2}浓度时，色度坐标从(0.527 5，0.369 5)变化到(0.606 3，0.353 2)，发光颜色由黄红向深红转变，色温从 1 580 K 降至 730 K。实验结果表明，通过调控两种离子的注入剂量可实现薄膜发光颜色的有效调控。

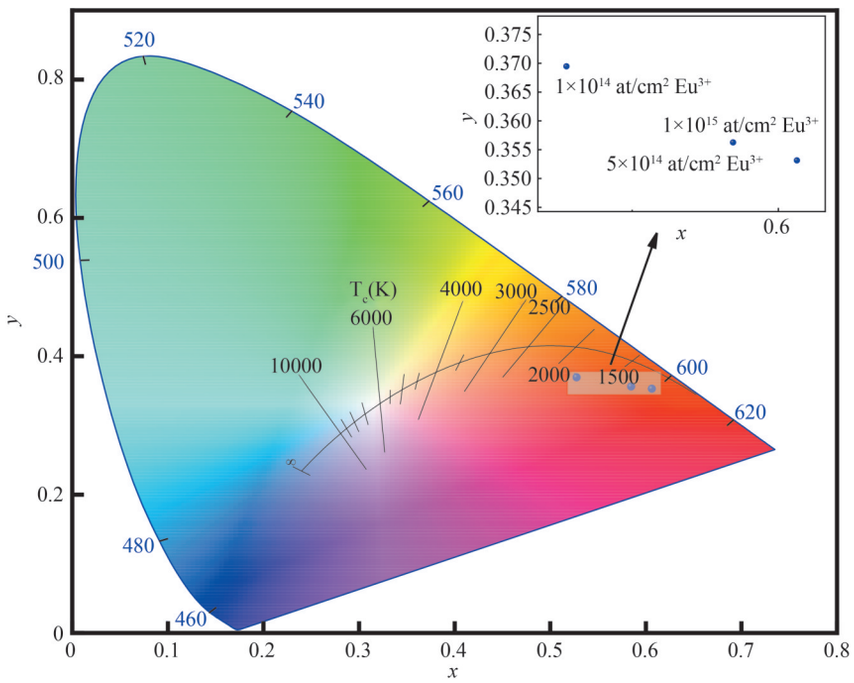


图 9 GaN:Sm^{3+}, Eu^{3+}发光色度图

Fig. 9 Chromaticity diagram of GaN:Sm^{3+},Eu^{3+} luminescence

表 3 不同剂量的Sm3+和Eu3+样品的CIE色度坐标和CCT

Table 3 CIE chromaticity coordinates and correlated color temperature (CCT) of samples doped with different concentrations of Sm^{3+} and Eu^{3+}

Samples (5×10^{14} at/cm^2 Sm^{3+})	CIE-x	CIE-y	CCT/K
1×10^{14} at/cm^2 Eu^{3+}	0.527 5	0.369 5	1 580
5×10^{14} at/cm^2 Eu^{3+}	0.584 5	0.356 3	820
1×10^{15} at/cm^2 Eu^{3+}	0.606 3	0.353 2	730

3 结论

本文通过离子注入制备了Sm^{3+}/Eu^{3+}共掺GaN薄膜,并系统研究了其结构与发光特性。拉曼光谱与高分辨X射线衍射分析表明,离子注入导致晶体质量下降,样品内部存在压应力,且压应力随注入剂量增加而增大。Sm^{3+}和Eu^{3+}的发光主峰分别位于578 nm ($^4G_{5/2}\rightarrow{}^6H_{5/2}$)和620 nm ($^5D_0\rightarrow{}^7F_2$)附近。计算表明,$Sm^{3+}$主要通过电偶极-电偶极、电偶极-电四极共振方式将能量单向传递给Eu^{3+},能量传递途径为$^4G_{5/2}$[Sm^{3+}]+$^7F_0$[Eu^{3+}]→$^6H_{5/2}$[Sm^{3+}]+$^5D_0$[Eu^{3+}]。样品的发光颜色可从黄红向深红转变,相关色温由1 580 K向730 K转变。通过调控Sm^{3+}和Eu^{3+}的浓度配比,可实现薄膜发光颜色的调控,这为开发基于GaN的红光LED提供了新的思路与实验依据。

参考文献

[1] JABBAR H D, FAKHRI M A, ABDULRAZZAQ M J. Gallium nitride - based photodiode: a review[J]. Materials Today: Proceedings, 2021, 42: 2829-2834.

[2] LI Yuzeng. Recent advances in GaN-based thin film materials and devices[J]. Semiconductor Technology, 1998, (3): 2-5.
李玉增. GaN基薄膜材料和器件的最新进展[J]. 半导体技术, 1998, (3): 2-5.

[3] MOHAMMAD S N, SALVADOR A A, MORKOC H. Emerging gallium nitride based devices[J]. Proceedings of the IEEE, 1995, 83(10): 1306-1355.

[4] AGGARWAL N, GUPTA G. Enlightening gallium nitride-based UV photodetectors[J]. Journal of Materials Chemistry C, 2020, 8(36): 12348-12354.

[5] LV S, WANG S, LI L, et al. Gallium nitride based electrode for high-temperature supercapacitors[J]. Advanced Science, 2023, 10(15): 2300780.

[6] UDABE A, BARAIA-ETXABURU I, DIEZ D G. Gallium nitride power devices: a state of the art review[J]. IEEE

Access, 2023, 11: 48628-48650.
[7] XUE D, SUN C T. 4f chemistry towards rare earth materials science and engineering[J]. Sci China-Technol Sci, 2017, 60(11): 1767-1768.
[8] NANDE A, RAUT S, DHOBLE S J. Charge transfer in rare-earth-doped inorganic materials[M]. Advanced Materials for Solid State Lighting. Singapore: Springer Nature Singapore, 2023: 31-58.
[9] CAROENA G, JUSTO J F, MACHADO W V M, et al. Rare-earth impurities in gallium nitride: The role of the Hubbard potential[J]. Diamond and Related Materials, 2012, 27: 64-67.
[10] LI Qianqian, HAO Qiuyan, LI Ying, et al. Theoretical study on electronic structure and optical properties of rare earth (Ce, Pr) doped GaN[J]. Acta Physica Sinica, 2013, 62(1): 385-392.
李倩倩，郝秋艳，李英，等. 稀土元素(Ce,Pr)掺杂GaN的电子结构和光学性质的理论研究[J]. 物理学报，2013, 62(1): 385-392.
[11] HALAMBALAKIS G, ROUSSEAU N, BRIOT O, et al. Growth and characterisation of Eu doped GaN thin films[J]. Superlattices and Microstructures, 2004, 36(4-6): 721-728.
[12] SAWAHATA J, BANG H, SEO J, et al. Optical processes of red emission from Eu doped GaN[J]. Science and Technology of Advanced Materials, 2005, 6(6): 644-648.
[13] WANG K, MARTIN R W, NOGALES E, et al. Optical properties of high-temperature annealed Eu-implanted GaN[J]. Optical Materials, 2006, 28(6-7): 797-801.
[14] NGO N H, NISHIKAWA A, FUJIWARA Y, et al. Investigation of optical gain in Eu-doped GaN thin film grown by OMVPE method[J]. Journal of Science: Advanced Materials and Devices, 2016, 1(2): 220-223.
[15] PERES M, MAGALHAES S, RODRIGUES J, et al. The role of the annealing temperature on the optical and structural properties of Eu doped GaN/AlN QD[J]. Optical Materials, 2011, 33(7): 1045-1049.
[16] LANG J H, WANG J, ZHANG Q, et al. Tunable bandgap and optical properties of (Eu, Sm) codoped ZnO nanoparticles[J]. Journal of Materials Science: Materials in Electronics, 2016, 27(10): 11034-11040.
[17] ELFAYOUMI M A K, FAROUK M, BRIK M G, et al. Spectroscopic studies of Sm^{3+} and Eu^{3+} co-doped lithium borate glass[J]. Journal of Alloys and Compounds, 2010, 492(1-2): 712-716.
[18] PAVITRA E, RAJU G S R, KO Y H, et al. A novel strategy for controllable emissions from Eu^{3+} or Sm^{3+} ions co-doped SrY_2O_4: Tb^{3+} phosphors[J]. Physical Chemistry Chemical Physics, 2012, 14(32): 11296-11307.
[19] LU Z, ZHANG K, ZHUANG J, et al. Recent progress of InGaN-based red light emitting diodes[J]. Micro and Nanostructures, 2023, 183: 207669.
[20] QADRI S B, MOLNAR B, YOUSUF M, et al. X-ray determination of strain in ion implanted GaN[J]. Nuclear Instruments and Methods in Physics Research Section B: Beam Interactions with Materials and Atoms, 2002, 190(1-4): 878-881.
[21] LINK A, BITZER K, LIMMER W, et al. Temperature dependence of the E_2 and A_1 (LO) phonons in GaN and AlN[J]. Journal of Applied Physics, 1999, 86(11): 6256-6260.
[22] ZENG Y, NING J, ZHANG J, et al. Raman analysis of E_2 (high) and A_1 (LO) phonon to the stress-free GaN grown on sputtered AlN/graphene buffer layer[J]. Applied Sciences, 2020, 10(24): 8814.
[23] TANG Jianjun, LIANG Ting, XIONG Jijun, et al. Raman spectroscopy analysis of stress state in heteroepitaxial Si/GaN[J]. Laser & Optoelectronics Progress, 2010, 47(8): 133-137
唐建军，梁庭，熊继军，等. 异质外延Si/GaN应力状态的拉曼光谱测试分析[J]. 激光与光电子学进展，2010, 47(8): 133-137.
[24] LEE I H, CHOI I H, LEE C R, et al. Stress relaxation in Si-doped GaN studied by Raman spectroscopy[J]. Journal of Applied Physics, 1998, 83(11): 5787-5791.
[25] LOZYKOWSKI H J, JADWISIENCZAK W M, BROWN I. Cathodoluminescence of GaN doped with Sm and Ho[J]. Solid State Communications, 1999, 110(5): 253-258.
[26] CHIANG C H, FANG Y C, LIN H Y, et al. Photoluminescence properties and thermal stability of samarium-doped barium phosphate phosphors[J]. Ceramics International, 2017, 43(5): 4353-4356.
[27] ZANATTA A R. Visible light emission and energy transfer processes in Sm-doped nitride films[J]. Journal of Applied Physics, 2012, 111(12): 123105.
[28] GRUBER J B, ZANDI B, LOZYKOWSKI H J, et al. Spectroscopic properties of Sm^{3+} ($4f^5$) in GaN[J]. Journal of Applied Physics, 2002, 91(5): 2929-2935.
[29] BI Changhong, MENG Qingyu. Luminescent properties and energy transfer mechanism of CaWO4:Sm3+ phosphors[J]. Acta Physica Sinica, 2013, 62(19): 197804.
毕长虹，孟庆裕. CaWO4: Sm^{3+}荧光粉的发光性质及其能量传递机理[J]. 物理学报，2013, 62(19): 197804.
[30] CHEN F F, XIA Y L, WANG X, et al. Raman scattering and cathodoluminescence properties of Er^{3+} and Eu^{3+} co-doped GaN films[J]. Journal of Luminescence, 2019, 206: 603-607.

[31] DEXTER D L, SCHULMAN J H. Theory of concentration quenching in inorganic phosphors[J]. The Journal of Chemical Physics, 1954, 22(6): 1063-1070.
[32] HUANG D, ZHOU Y, XU W, et al. Photoluminescence properties of M^{3+} (M^{3+}= Bi^{3+}, Sm^{3+}) activated $Na_5Eu(WO_4)_4$ red-emitting phosphors for white LEDs[J]. Journal of Alloys and Compounds, 2013, 554: 312-318.
[33] VAN UITERT L G. Energy transfer between rare earth ions in tungstates[J]. Journal of Luminescence, 1971, 4(1): 1-7.
[34] MCCAMY C S. Correlated color temperature as an explicit function of chromaticity coordinates[J]. Color Research & Application, 1992, 17(2): 142-144.
[35] BRITO S L, LODI T A, MUNIZ R F, et al. Energy transfer investigation of Sm^{3+}/Eu^{3+} CaBAl glasses[J]. Journal of Luminescence, 2020, 219: 116947.
[36] LIN H Y, FANG Y C, CHU S Y. Energy transfer Sm^{3+}→Eu^{3+} in potential red phosphor $(Ca, Ba)_3(VO_4)_2$:Sm^{3+},Eu^{3+} for use in organic solar cells and white light-emitting diodes[J]. Journal of the American Ceramic Society, 2010, 93(11): 3850-3856.

Structural and Luminescence Properties of Sm^{3+} and Eu^{3+} Co-doped GaN Thin Films

XU Da[1], WANG Xiaodan[1], SHU Zhengdong[1], ZHAO Chengwei[1], MAO Hongmin[1], GAO Xiaodong[2], ZHENG Shunan[2], ZENG Xionghui[2]

(1 *Key Laboratory of Intelligent Optoelectronic Devices and Chips of Jiangsu Higher Education Institutions, School of Physical Science and Technology, Suzhou University of Science and Technology, Suzhou* 215009, *China*)
(2 *Suzhou Institute of Nano-Tech and Nano-Bionics, Chinese Academy of Sciences, Suzhou* 215123, *China*)

Abstract: Gallium nitride (GaN) is a cornerstone of third-generation wide-bandgap semiconductor technology, valued for its exceptional electronic mobility, thermal stability, chemical inertness, and robustness under extreme operating conditions. These qualities have driven its adoption in high-power electronics, high-frequency devices, and ultraviolet optoelectronics. However, a persistent challenge in GaN-based photonics is achieving efficient and stable red emission. Conventional InGaN-based red Light-Emitting Diodes (LEDs) suffer from efficiency droop and phase separation issues inherent to the high indium (In) content required for red wavelengths. As an alternative, doping GaN with rare-earth (RE) ions—which exhibit sharp, stable intra-4f shell emissions largely independent of the host matrix—offers a promising route to high-color-purity red light. Among these, trivalent europium ions (Eu^{3+}) are renowned for their intense red emission lines around 620 nm. To enhance the optical activation and emission efficiency of such RE centers, co-doping with a sensitizer ion is a widely employed strategy. Samarium ions (Sm^{3+}) have demonstrated effective sensitization of Eu^{3+} luminescence in various host materials through resonant energy transfer. Nevertheless, the specific system of Sm^{3+}/Eu^{3+} co-doped GaN is still in its infancy. This study aims to systematically investigate the structural modifications and luminescence characteristics—particularly the energy transfer dynamics—in GaN thin films co-doped with Sm^{3+} and Eu^{3+} ions, thereby evaluating its potential as a novel red-emitting material platform compatible with established GaN semiconductor processes.

This research employed ion implantation as the doping technique to introduce Sm^{3+} and Eu^{3+} ions into high-quality GaN thin films grown on c-plane sapphire substrates via metal-organic chemical vapor deposition (MOCVD). A series of samples were prepared: including Sm^{3+} single-doped samples with varying doses (1×10^{14}, 5×10^{14}, 1×10^{15} at/cm^2), and Sm^{3+}/Eu^{3+} co-doped samples with a fixed Sm^{3+} dose (5×10^{14} at/cm^2) and varying Eu doses (1×10^{14}, 5×10^{14}, 1×10^{15} at/cm^2). Post-implantation thermal annealing at 1 000 ℃ in an ammonia atmosphere was conducted to recover implantation-induced lattice damage and to optically activate the RE ions. The structural integrity and stress state of the doped films were comprehensively assessed using High-resolution X-ray Diffraction (HRXRD) and Raman spectroscopy. The optical emission properties were investigated using Cathodoluminescence (CL) spectroscopy.

HRXRD rocking curve analysis of the GaN (0002) plane revealed that the Full Width at Half Maximum (FWHM) increased with higher Sm^{3+} concentrations in single-doped samples, indicating a degradation of

crystalline quality due to implantation-induced defects. In co-doped samples with a fixed Sm^{3+} dose, the FWHM exhibited a complex, non-monotonic trend as the Eu^{3+} dose increased, showing a slight initial decrease followed by a rise at higher doses. This suggests that the incorporation of a low dose of Eu^{3+} may induce minor lattice distortions that slightly improve local ordering, while higher doses exacerbate defect formation. Lattice constant analysis from $2\theta/\omega$ scans and Raman shift measurements of the E_2^{high} phonon mode provided consistent evidence of stress evolution. Sm^{3+} single-doping introduced tensile stress, whereas the introduction of Eu^{3+} in co-doped samples led to a significant increase in compressive stress, which intensified with higher Eu^{3+} doses.

Cathodoluminescence spectroscopy provided clear evidence of efficient energy transfer from Sm^{3+} (sensitizer) to Eu^{3+} (activator). In Sm^{3+} single-doped samples, characteristic emission peaks were observed from Sm^{3+} at approximately 577 nm ($^4G_{5/2} \rightarrow {}^6H_{5/2}$), 618 nm ($^4G_{5/2} \rightarrow {}^6H_{7/2}$), and 666 nm ($^4G_{5/2} \rightarrow {}^6H_{7/2}$). In the co-doped samples, the Sm^{3+} emission intensity, particularly the 577 nm peak, was significantly quenched, while the characteristic Eu^{3+} emission lines, especially the dominant red emission at ~620 nm ($^5D_0 \rightarrow {}^7F_2$), were strongly enhanced with increasing Eu^{3+} concentration. This anti-correlation provides clear evidence for a non-radiative energy transfer process. The primary energy transfer pathway was identified as $^4G_{5/2}$ (Sm^{3+}) + $^7F_0$ (Eu^{3+}) → $^6H_{5/2}$ (Sm^{3+}) + $^5D_0$ (Eu^{3+}), favored by the near-perfect resonance (energy mismatch of only ~74 meV) between the Sm^{3+} $^4G_{5/2} \rightarrow {}^6H_{5/2}$ transition and the Eu^{3+} $^7F_0 \rightarrow {}^5D_0$ absorption.

Further quantitative analysis based on Dexter′s theory was conducted to elucidate the dominant interaction mechanism. By analyzing the dependence of the Sm^{3+} emission quenching ratio on the total RE concentration through fitting, it was determined that energy transfer occurs primarily via electric dipole-dipole and electric dipole-quadrupole interactions. Critical energy transfer distances (R_c) were calculated to lie between 1.66 nm and 2.24 nm for the studied concentration range, confirming the feasibility of efficient resonant transfer at these doping levels.

The impact of co-doping on the emitted light color was evaluated using the Commission Internationale de l′Éclairage (CIE) chromaticity coordinates. As the Eu^{3+} dose increased from 1×10^{14} to 1×10^{15} at/cm^2, the CIE coordinates systematically shifted from (0.527 5, 0.369 5) in the yellowish-red region to (0.606 3, 0.353 2) in the deep red region. Correspondingly, the calculated Correlated Color Temperature (CCT) decreased from 1 580 K to 730 K. This demonstrates that by adjusting the concentration of Eu^{3+} relative to the fixed proportion of the Sm^{3+} sensitizer, a clear and controllable tuning of the emission color toward saturated red can be achieved.

In conclusion, this study successfully fabricated and characterized Sm^{3+}/Eu^{3+} co-doped GaN thin films via ion implantation. Although the doping process introduces compressive stress and affects the crystalline quality, it enables efficient resonant energy transfer from Sm^{3+} to Eu^{3+}. This transfer effectively pumps the Eu^{3+} $^5D_0$ level, resulting in intensified red emission around 620 nm. Most notably, the emission color can be tuned from yellowish-red to deep red by varying the Eu^{3+} concentration, providing a direct means to achieve targeted red chromaticity. These findings offer foundational experimental insights and a material processing framework for developing GaN-based red-emitting devices utilizing the Sm^{3+}/Eu^{3+} co-doping scheme, presenting a potentially advantageous alternative to high-In-content InGaN for red micro-LEDs and other advanced optoelectronic applications. Future work may focus on optimizing implantation and annealing parameters to mitigate structural damage and further enhance the luminescence efficiency of this co-doped system.

Key words: Gallium nitride (GaN); Europium ions (Eu^{3+}); Energy transfer; Samarium ions (Sm^{3+}); Cathodoluminescence

OCIS Codes: 310.6860; 310.6188; 310.3840; 240.6490

CSTR: 32255.14.gzxb20265501.0131003

Foundation item: National Natural Science Foundation of China (61974158), Natural Science Fund of Jiangsu Province (BK20221263), Jiangsu Key Disciplines of the Fourteenth Five-Year Plan (2021135)